JACS
JOURNAL OF THE AMERICAN CHEMICAL SOCIETY

Communication

pubs.acs.org/JACS

CuTe Nanocrystals: Shape and Size Control, Plasmonic Properties, and Use as SERS Probes and Photothermal Agents

Wenhua Li,[†] Reza Zamani,[†,⊥] Pilar Rivera Gil,[∥] Beatriz Pelaz,[∥] Maria Ibáñez,[‡] Doris Cadavid,[†] Alexey Shavel,[†] Ramon A. Alvarez-Puebla,[#,∇,§] Wolfgang J. Parak,[∥] Jordi Arbiol,[⊥,§] and Andreu Cabot*[,†,‡]

[†]Catalonia Energy Research Institute−IREC, Barcelona 08930, Spain

[⊥]Institut de Ciència de Materials de Barcelona, ICMAB-CSIC, Campus de la UAB, Bellaterra 08193, Spain

[∥]Philipps Universität Marburg, 35037 Marburg, Germany

[‡]Departament d'Electrònica, Universitat de Barcelona, Barcelona 08028, Spain

[#]Department of Electronic Engeneering, Universitat Rovira i Virgili, Tarragona 43007, Spain

[∇]Center for Chemical Technology of Catalonia, Tarragona 43007, Spain

[§]Institució Catalana de Recerca i Estudis Avançats, 08010 Barcelona, Spain

Supporting Information

ABSTRACT: We report a procedure to prepare highly monodisperse copper telluride nanocubes, nanoplates, and nanorods. The procedure is based on the reaction of a copper salt with trioctylphosphine telluride in the presence of lithium bis(trimethylsilyl)amide and oleylamine. CuTe nanocrystals display a strong near-infrared optical absorption associated with localized surface plasmon resonances. We exploit this plasmon resonance for the design of surface-enhanced Raman scattering sensors for unconventional optical probes. Furthermore, we also report here our preliminary analysis of the use of CuTe nanocrystals as cytotoxic and photothermal agents.

Copper-based chalcogenides are used in a wide range of applications, from thermoelectrics to batteries, including photonics, photovoltaics, and photothermal therapy.[1,2] They are usually p-type semiconductors, due to the presence of copper vacancies. Copper vacancies not only determine charge transport properties but also provide copper chalcogenides with a particularly attractive property: a composition-dependent localized surface plasmon resonance (LSPR) in the near-infrared (NIR).[3] In particular, copper telluride is characterized by a large thermal power, a direct band gap between 1.1 and 1.5 eV, and superionic conductivity. Copper telluride can exist in a wide range of compositions and phases, which allows tuning its properties by just adjusting the Cu:Te ratio. These properties provide it with both high fundamental interest and technological potential. However, in spite of its relevance, little is known about its properties at the nanoscale, e.g., plasmonics, and a synthetic route to produce uniform copper telluride nanoparticles (NPs) is yet to be reported. While a variety of procedures to prepare sulfide and selenide NPs with excellent uniformity are available,[3,4] one main constraint to produce telluride NPs and particularly copper telluride is the reduced number of tellurium sources available, which narrows the range of accessible reaction conditions to direct telluride NPs nucleation and growth.

In the present work, we demonstrate the potential of lithium bis(trimethylsilyl)amide to control the growth of copper telluride NPs and detail a simple synthetic route to produce highly uniform copper telluride nanocubes, nanoplates, and nanorods. We further demonstrate how copper telluride NPs provide a new and unique optical platform for the design of plasmonic sensors of a wide family of molecules that cannot be conventionally analyzed with surface-enhanced Raman scattering (SERS).[5] Furthermore, we report preliminary results on the use of copper telluride NPs for photothermal destruction of cells.

Copper telluride NPs were prepared by reacting copper(I) chloride with trioctylphosphine telluride (TOPTe) in the presence of trioctylphosphine (TOP), trioctylphosphine oxide (TOPO), lithium bis(trimethylsilyl)amide ($LiN(SiMe_3)_2$), and oleylamine (OLA). In a typical synthesis, 0.25 mmol of CuCl was mixed with 1 mmol of TOPO and 6 mL of OLA in a 25 mL three-neck flask. The mixture was heated under vacuum to 100 °C to obtain a clear blue solution and kept at this temperature for 30 min to remove low-boiling-point impurities. The temperature was then increased to 160 °C, and 0.125 mL of TOP was added. In parallel, a tellurium precursor solution was prepared inside a glovebox by mixing 0.125 mL of a 2 M TOPTe solution with 0.5 mL of a 0.5 M $LiN(SiMe_3)_2$ solution in dried octadecene (ODE). The tellurium solution was rapidly injected into the copper solution maintained at 160 °C. Upon injection, the solution color immediately changed to deep green, and the temperature dropped to 152 °C. Just after injection, the temperature was set to 220 °C, and NPs were allowed to grow for 30 min. During cooling, when the temperature reached 70 °C, 2 mL of oleic acid was added to replace the weakly bound OLA molecules.

Figure 1A shows representative transmission electron microscopy (TEM) and high-resolution TEM (HRTEM) micrographs of the copper telluride NPs obtained by the procedure described above. NPs displayed a cubic geometry

Received: February 7, 2013
Published: April 30, 2013

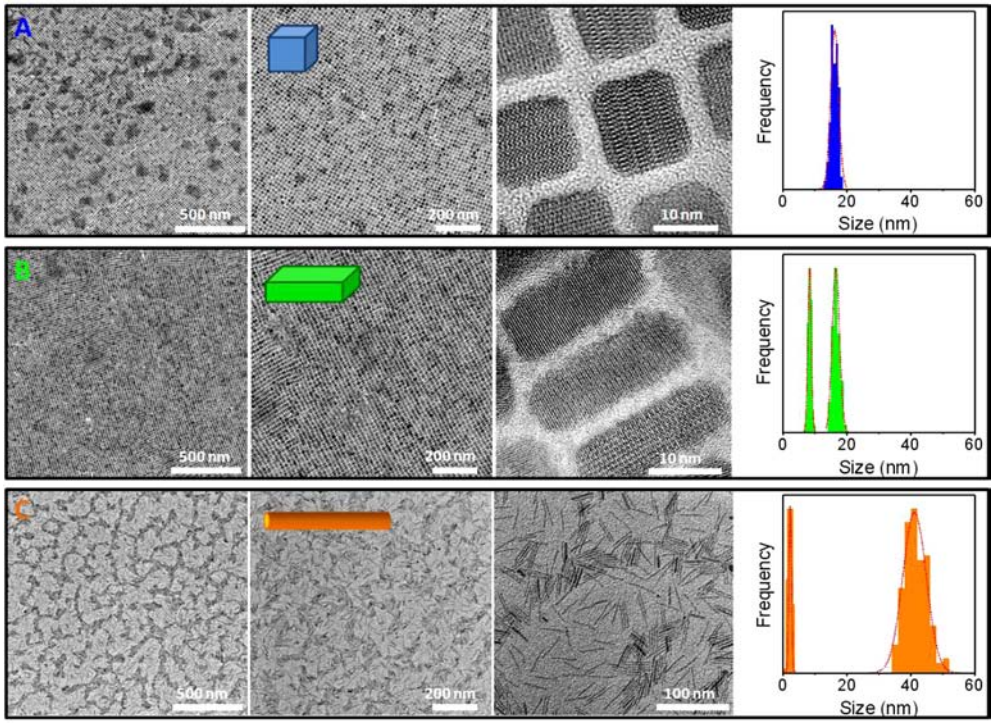

Figure 1. TEM micrograph and size distribution histograms of CuTe NPs: (A) nanocubes, (B) nanoplates, and (C) nanorods.

and very narrow size distributions (<5%), which facilitated their self-assembly into cubic superlattices extending several micrometers.

The presence of $LiN(SiMe_3)_2$ molecules was found critical to produce cubic NPs with narrow size distributions. When we attempted to produce copper telluride NPs without this compound, large rectangular plates with very broad size distributions were obtained (Figure S2). At the same time, without the presence of $LiN(SiMe_3)_2$, the reaction of $CuN(SiMe_3)_2$ with TOPTe resulted in quasi-spherical NPs (Figure S2). Following recent findings on the mechanism of formation of metal NPs in the presence of $LiN(SiMe_3)_2$ and OLA,[6] we speculate that $LiN(SiMe_3)_2$ activates the formation of a Cu−oleylamido complex, which is the actual species reacting with TOPTe to form the copper telluride NPs. Besides, the Cu−oleylamido complexes and/or lithium oleylamine may stabilize the NP surface during growth.

The Cu:Te nominal ratio, the reaction time and temperature, and the concentration of TOP were key parameters to control the size and shape of the copper telluride NPs obtained. By tuning the Cu:Te ratio, we could control the size of the nanocubes in the range between 10 and 20 nm (Figure S3). Nanocube size increased with the Cu:Te ratio. We hypothesize that TOPTe concentration controls NP nucleation. When the concentration of TOPTe was increased, a higher nucleation rate was initially obtained, reducing the total amount of precursor for posterior NP growth. Thus, smaller NPs were ultimately obtained.

When the reaction temperature was decreased from 220 °C to 190 °C and the growth time to 15 min, highly homogeneous copper telluride nanoplates were produced (Figures 1B, S4−S6). On the other hand, an increase of the TOP concentration resulted in the formation of nanorods. When 0.75 mL of TOP was added instead of 0.125 mL, the growth temperature set to 190 °C, and the growth time set to 2 min, thin nanorods were obtained (Figure 1C). By increasing the reaction time, thicker nanorods were produced but the size distribution worsened (Figure S7).

Energy-dispersive X-ray spectroscopy (EDX) and electron energy loss spectroscopy (EELS) analysis showed the NPs to have a Cu:Te atomic ratio close to 1:1 (Figure S8). Further single-particle analysis demonstrated the homogeneous distribution of the two elements within each particle and a very uniform composition from particle to particle (Figure S9).

Crystal phase identification in copper chalcogenides and more generally in transition metal chalcogenides is a challenging task. The partially filled d-shell in transition metals allows them to adopt multiple oxidation states, which results in compounds with large composition and structural diversity. Copper tellurides exist as orthorhombic CuTe, hexagonal Cu_2Te, Cu_3Te_4, Cu_7Te_5, etc. and also as nonstoichiometric $Cu_{2-x}Te$ phases.[7] X-ray diffraction (XRD) analyses demonstrated CuTe nanorods, nanocubes, and nanoplates to have the same crystal structure, but it did not allow us to unequivocally determine the structure, as the patterns measured did not exactly match with any of the copper telluride phases in the literature (Figure 2A).

Figures 1 and S10 show HRTEM micrographs of the CuTe nanocubes and nanoplates obtained. No reliable HRTEM micrograph could be obtained from nanorods due to electron-beam-induced structural modifications. From the HRTEM analysis, we associate the NP crystal phase with a tetragonal $Cu_{1.25}Te$ structure having cell parameters $a = b = 7.50 \pm 0.05$ Å and $c = 7.65 \pm 0.05$ Å. CuTe NPs further display a superstructure with periodicity of three unit cells, which could originate from an internal ordering of copper vacancies (Figure S10).[8]

Figure 2B shows the UV/vis spectra of colloidal CuTe NPs with different geometries. A strong absorption band centered at 900 nm and associated with LSPR[3a] is clearly observed in the

dx.doi.org/10.1021/ja401428e | J. Am. Chem. Soc. 2013, 135, 7098−7101

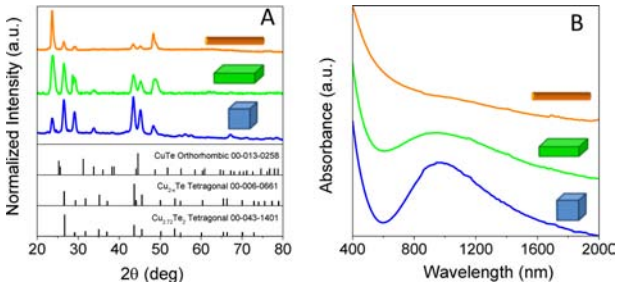

Figure 2. (A) XRD patterns and (B) UV/vis spectra of copper telluride nanocubes, nanoplates, and nanorods.

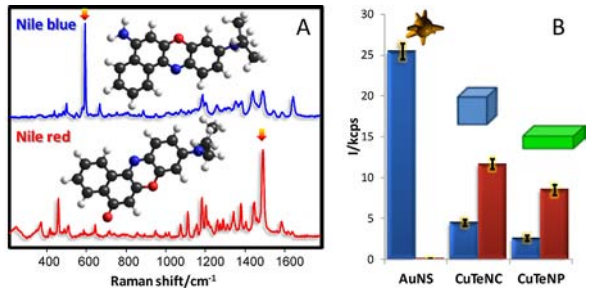

Figure 3. (A) SERS spectra of Nile blue and Nile red. (B) Comparison of the signal enhancement when using gold nanostars (AuNS), CuTe nanocubes (CuTeNC), and CuTe nanoplates (CuTeNP).

spectra obtained from CuTe nanocubes. This band had a weaker intensity in CuTe nanoplates and nearly disappeared from the UV/vis spectra of thin CuTe nanorods, probably because the small transversal dimension of thin nanorods does not support a detectable plasmon.

Plasmonic NPs find applications in a broad range of fields, from optoelectronics to biomedicine. A particularly interesting application is the use of their extremely high near-electric fields to increase the signals of molecules close to their surfaces. SERS spectroscopy is one of the most powerful techniques for ultradetection. Unfortunately, the direct applicability of this technique has been so far restricted to molecular families carrying functional groups ($-NH_2$ or $-SH$) with affinity for gold or silver, the most common plasmonic nanostructures. The analysis of other compounds requires of surface functionalization with trapping species which many times are difficult and expensive to obtain.[5] Thus, the preparation of plasmonic materials with different surface chemistry permits the direct identification of chemical families that present oxygen-based functional groups and that are ubiquitous in the environment and biological media as pollutants, metabolites, or disease markers.

On the other hand, small gold and silver NPs present LSPRs in the visible region, although it is possible to tune the size and shape of gold to shift these bands to the IR, as in the case of nanostars or nanoshells. This usually results in an increase in the particle size, limiting the applicability of these particles in living organisms. Notably, the natural excitation of CuTe LSPRs in the NIR paves the way for the improvement of bioapplications in either therapy or sensing.

CuTe NPs were analyzed without any analyte to check for surfactant spurious bands. Notably, at the normal experimental SERS conditions, TOPO and OLA did not yield any appreciable signal, consistent with the low SERS cross sections of aliphatic species (Figure S12). To probe the efficiency of the prepared CuTe particles as SERS sensors, two analytes were selected: Nile blue, which carries an ionized amino group, and Nile red, a highly hydrophobic molecule that has a keto-oxygen available for surface reaction. To compare the results of CuTe with gold nanostructures, gold nanostars—the most efficient nanostructure to date[9]—were also tested under the same conditions. Figure 3 shows the SERS spectra of Nile blue and Nile red and the enhancement factors for both analytes obtained with gold nanostars and CuTe nanocubes and nanoplates. The CuTe nanorods did not yield any SERS signal, which is consistent with their very weak plasmon peak. The other two, nanocubes and nanoplates, yielded good signal-to-noise spectra with enhancement factors of 1.5×10^6 and 10^6, respectively (Figure S14), for the hydrophobic Nile red. This is explained in light of both the copper chemistry and the hydrophobicity of the NPs. The Nile blue is a charged molecule; thus, despite the high affinity of the primary amines for copper, the electrostatic repulsion derived from the analyte charge inhibits the close contact of the target molecule with the surface. In the case of Nile red, its hydrophobicity and the tendency for the oxygen-containing groups to react with copper lead to a much more efficient retention, with a subsequent increase in the SERS signal. Notably, cubes offer a slightly higher signal as compared with plates. This phenomenon can be explained in terms of shape and plasmon concentration at the corners, which localize the LSPR, providing extremely high signals. However, the fact that the corners of the cubes are not perfectly shaped reduces this extra enhancement as compared with the plates. Further, comparison of the CuTe nanostructures with the gold nanostars showed that, although the amino-containing molecule gave a considerable higher signal with gold, due to both the photonic efficiency of gold nanostars and the perfect matching between the negatively charged gold surface and the positively charged amino group, Nile red could only be detected with CuTe due to the low affinity of ketones for gold.

Another major application of plasmonic NPs is in photothermal therapy. Photothermal therapy uses the local heat produced by plasmonic NPs when absorbing light to kill cancerous cells, which are sensitive to small temperature changes.[10,11] Hyperthermia therapies[10,12] are mostly used together with more conventional therapies such as radiotherapy or chemotherapy.

Gold NPs are typically used for photothermal therapy.[10] In spite of their toxicity, silver NPs have been also proposed for this application. The advantage of using silver instead of gold is that, to destroy cancerous cells, one can combine the intrinsic toxicity of silver NPs with their ability to increase the local temperature of the tissue.[11] This is, of course, a relative advantage, as the administration of toxic NPs would require a very careful localization in order to not affect healthy cells. NPs with a strong absorption band in the NIR are particularly interesting, because at these frequencies light can penetrate through cells and tissues, interacting only with cells containing the NPs, while at other wavelengths strong absorption by tissue occurs.

Copper sulfide and copper selenide have also been proposed recently as photothermal agents.[2] Copper telluride is a new candidate material whose potential is worth testing. For a preliminary study of the potential of CuTe NPs as photothermal agents, CuTe nanocubes were stabilized in water by coating them with an amphiphilic polymer (Supporting Information).[13] The polymer-coated CuTe NPs were extremely stable in water, and no agglomeration was detected during

dx.doi.org/10.1021/ja401428e | J. Am. Chem. Soc. 2013, 135, 7098−7101

periods of over a month. A solution of polymer-coated CuTe nanocubes was used to incubate 3T3 embryonic fibroblasts. After incubation, cells were placed in a solution of 4′,6-diamidino-2-phenylindole (DAPI). DAPI is a dye which slowly permeates living cells, but its penetration is highly increased when the plasma and nuclear membranes are damaged. Figure 4 shows transmission and fluorescent images of untreated cells

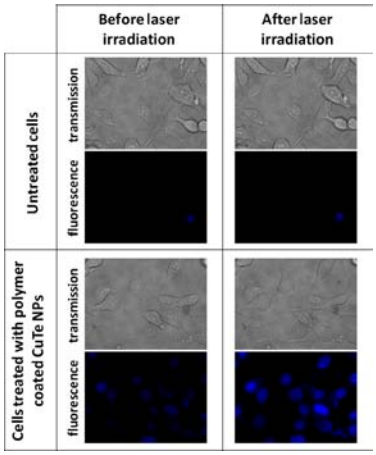

Figure 4. CuTe nanocubes-induced disruption of cell viability.

and those containing CuTe nanocubes before and after 830 nm NIR laser irradiation. An increase in the fluorescence intensity of the nucleus is a result of plasma and nuclear membrane damage, which in turn indicates disruption of cell viability. As can be seen in Figure 4, only cells containing the nanocubes were dying. A certain degree of toxicity can be seen, as some cells were dying before laser irradiation. This could be due to oxidation of the CuTe NP surface, which would lead to the release of toxic ions. Nevertheless, a significantly higher degree of toxicity was assessed after laser irradiation. These preliminarily results point out that copper telluride could be used as a cytotoxic and photothermal agent. Compared to silver, CuTe NPs have the advantage of displaying their plasmon peak in the NIR, which would allow for selectively targeting NP-labeled cancer cells without affecting unlabeled cells, although again, their intrinsic toxicity would require a very localized administration or a more efficient encapsulation.[11]

In summary, we obtained highly uniform CuTe nanocubes, nanoplates, and nanorods in the presence of $LiN(SiMe_3)_2$. CuTe NPs show a strong plasmonic peak at 900 nm, which allows their use as SERS probes and in photothermal therapy. While CuTe NPs are not competitive with those of gold for the detection of conventional analytes, they find good applicability for the direct ultradetection of oxygen-substituted targets. On the other hand, CuTe nanocubes induced a high degree of toxicity by locally increasing the temperature and possibly by releasing toxic ions to the cellular environment.

■ ASSOCIATED CONTENT

Supporting Information

Additional characterization, and procedures followed for SERS measurements, polymer coating, and photothermal experiments. This material is available free of charge via the Internet at http://pubs.acs.org.

■ AUTHOR INFORMATION

Corresponding Author

acabot@irec.cat

Notes

The authors declare no competing financial interest.

■ ACKNOWLEDGMENTS

This research was supported by the European Regional Development Funds. J.A. and R.Z. acknowledge MAT2010-15138. Part of this work was supported by HFSP grant RGP0052/2012 to W.J.P.

■ REFERENCES

(1) (a) Zhao, Y.; Burda, C. *Energy Environ. Sci.* **2012**, *5*, 5564−5576. (b) Ibáñez, M.; Cadavid, D.; Zamani, R.; García-Castelló, N.; Izquierdo-Roca, V.; Li, W.; Fairbrother, A.; Prades, J. D.; Shavel, A.; Arbiol, J.; Pérez-Rodríguez, A.; Morante, J. R.; Cabot, A. *Chem. Mater.* **2012**, *24*, 562−570. (c) Ibáñez, M.; Zamani, R.; Li, W.; Cadavid, D.; Gorsse, S.; Katcho, N. A.; Shavel, A.; López, A. M.; Morante, J. R.; Arbiol, J.; Cabot, A. *Chem. Mater.* **2012**, *24*, 4615−4622.

(2) (a) Hessel, C. M.; Pattani, V. P.; Rasch, M.; Panthani, M. G.; Koo, B.; Tunnell, J. W.; Korgel, B. A. *Nano Lett* **2011**, *11*, 2560−2566. (b) Tian, Q.; Jiang, F.; Zou, R.; Liu, Q.; Chen, Z.; Zhu, M.; Yang, S.; Wang, J.; Wang, J.; Hu, J. *ACS Nano* **2011**, *5*, 9761−9771. (c) Li, Y.; Lu, W.; Huang, Q.; Li, C.; Chen, W. *Nanomedicine* **2010**, *5*, 1161−1171.

(3) (a) Kriegel, I.; Jiang, C.; Rodríguez-Fernández, J.; Schaller, R. D.; Talapin, D. V.; da Como, E.; Feldmann, J. *J. Am. Chem. Soc.* **2012**, *134*, 1583−1590. (b) Luther, J. M.; Jain, P. K.; Ewers, T.; Alivisatos, A. P. *Nat. Mater.* **2011**, *10*, 361−366. (c) Dorfs, D.; Härtling, T.; Miszta, K.; Bigall, N. C.; Kim, M. R.; Genovese, A.; Falqui, A.; Povia, M.; Manna, L. *J. Am. Chem. Soc.* **2011**, *133*, 11175−11180.

(4) (a) Li, W.; Shavel, A.; Guzman, R.; Rubio-Garcia, J.; Flox, C.; Fan, J.; Cadavid, D.; Ibáñez, M.; Arbiol, J.; Morante, J. R.; Cabot, A. *Chem. Commun.* **2011**, *47*, 10332−10334. (b) Li, W.; Zamani, R.; Ibáñez, M.; Cadavid, D.; Shavel, A.; Morante, J. R.; Arbiol, J.; Cabot, A. *J. Am. Chem. Soc.* **2013**, *135*, 4664−4667.

(5) (a) Alvarez-Puebla, R. A.; Liz-Marzan, L. M. *Chem. Soc. Rev.* **2012**, *41*, 43−51. (b) Alvarez-Puebla, R. A.; Liz-Marzan, L. M. *Angew. Chem., Int. Ed.* **2012**, *51*, 11214−11223.

(6) Kravchyk, K.; Protesescu, L.; Bodnarchuk, M. I.; Krumeich, F.; Yarema, M.; Walter, M.; Guntlin, C.; Kovalenko, M. V. *J. Am. Chem. Soc.* **2013**, *135*, 4199−4202.

(7) (a) Neyvasagam, K.; Soundararajan, N.; Venkatraman, V.; Ganesan, V. *Vacuum* **2007**, *82*, 72−77. (b) Sridhar, K.; Chattopadhyay, K. *J. Alloys Compd.* **1998**, *264*, 293−298. (c) Li, B.; Xie, Y.; Huang, J.; Liu, Y.; Qian, Y. *Chem. Mater.* **2000**, *12*, 2614−2616.

(8) Silva, J. L. F. D.; Wei, S.-H.; Zhou, J.; Wu, X. *Appl. Phys. Lett.* **2007**, *91*, 091902.

(9) Rodríguez-Lorenzo, L.; Álvarez-Puebla, R. A.; Pastoriza-Santos, I.; Mazzucco, S.; Stéphan, O.; Kociak, M.; Liz-Marzán, L. M.; García de Abajo, F. J. *J. Am. Chem. Soc.* **2009**, *131*, 4616−4618.

(10) Pelaz, B.; Grazu, V.; Ibarra, A.; Magen, C.; del Pino, P.; de la Fuente, J. M. *Langmuir* **2012**, *28*, 8965−8970.

(11) Di Corato, R.; Palumberi, D.; Marotta, R.; Scotto, M.; Carregal-Romero, S.; Rivera-Gil, P.; Parak, W. J.; Pellegrino, T. *Small* **2012**, *8*, 2731−2742.

(12) Martínez-Boubeta, C.; et al. *Sci. Rep.* **2013**, *3*, 1652.

(13) (a) Pellegrino, T.; Manna, L.; Kudera, S.; Liedl, T.; Koktysh, D.; Rogach, A. L.; Keller, S.; Radler, J.; Natile, G.; Parak, W. J. *Nano Lett.* **2004**, *4*, 703−707. (b) Zhang, F.; Lees, E.; Amin, F.; Rivera-Gil, P.; Yang, F.; Mulvaney, P.; Parak, W. J. *Small* **2011**, *7*, 3113−3127.